Water balance changes in response to climate change in the upper Hailar River Basin, China

Junfang Liu, Baolin Xue, Yinglan A, Wenchao Sun and Qingchun Guo

ABSTRACT

Projected climate change will have a profound effect on the hydrological balance of river basins globally. Studying water balance modification under changing climate conditions is significant for future river basin management, especially in certain arid and semiarid areas. In this study, we evaluated water balance changes (1981–2011) in the upper Hailar River Basin on the Mongolian Plateau. To evaluate the hydrological resilience of the basin to climate change, we calculated two Budyko metrics, i.e. dynamic deviation (d) and elasticity (e). The absolute magnitude of d reflects the ability of a basin to resist the influence of climate change and maintain its stable ecological function, whereas parameter e is used to assess whether a basin is hydrologically elastic. Results revealed modification of the hydrological balance during the study period has manifested as a decreasing trend of runoff and runoff-precipitation ratio. Correspondingly, basin-averaged evapotranspiration has also shown a decreasing trend, attributable mainly to precipitation. Furthermore, the calculated elasticity ($e = 8.03$) suggests the basin has high hydrological resilience, which indicates the basin ecosystem may maintain its hydrological function to a certain extent under a changing climate. The results of this study could assist water resource management in the study area and the prediction of ecosystem response to future climate change.

Key words | Budyko curve, climate change, Hailar River Basin, resilience, resistance, water balance

Junfang Liu
Baolin Xue (corresponding author)
Yinglan A
Wenchao Sun
College of Water Sciences,
Beijing Normal University,
Beijing 100875,
China
E-mail: *xuebl@bnu.edu.cn*

Baolin Xue
Wenchao Sun
Beijing Key Laboratory of Urban Hydrological Cycle and Sponge City Technology,
Beijing,
China

Qingchun Guo
School of Environment and Planning,
Liaocheng University,
Liaocheng, 252000,
China

HIGHLIGHTS

- Water balance changes (1981–2011) in the upper Hailar River Basin on the Mongolian Plateau were investigated.
- The hydrological balance during the study period has manifested as a trend of decrease of runoff and a decreased runoff–precipitation ratio.
- The calculated elasticity (e = 8.03) suggests the basin has high hydrological resilience, which indicates the basin ecosystem might maintain its hydrological function to a certain extent under a changing climate.

INTRODUCTION

The arid and semiarid areas that cover >50% of China's national mainland territory are distributed primarily on the Tibetan Plateau and in northern China. Grassland is the main vegetation type in such regions that are usually subjected to water limitations and intense effects associated with climate warming (Fang *et al.* 2018a; Han *et al.* 2018a; A *et al.* 2019b). Therefore, arid and semiarid areas are ecologically vulnerable and sensitive to climate extremes (Miao

doi: 10.2166/nh.2020.032

et al. 2014; Fang et al. 2018b). Moreover, vegetation transpiration accounts for a large proportion of the total evapotranspiration in arid and semiarid regions and thus it plays an essential role in the regional hydrological balance (Han et al. 2018a; Wang et al. 2018a; A et al. 2019a). Research has shown that drought in arid and semiarid areas is projected to become intensified in the future, which could trigger considerable change in the processes of the hydrological balance and affect regional water resources (Dai 2011; Wang et al. 2019a). Therefore, it is of critical importance to study the modification of the water balance under the effects of climate change in arid and semiarid regions to ensure sustainable water resources management.

Projected global climate change in the 21st century could have a considerable effect on the hydrological balance of many river basins, especially in certain arid and semiarid regions, in terms of important variables such as precipitation, runoff, and evaporation (Cuo et al. 2013; Zhang et al. 2016; Wang et al. 2019b). Earlier studies have investigated changes of the hydrological balance due to climate change in many river basins of northern China. In the middle section of the Yellow River Basin, both streamflow and precipitation have exhibited downward trends and evaporation has presented an upward trend during the previous 60 years (He et al. 2013; Bao et al. 2019). Cuo et al. (2013) analyzed observed streamflow changes in the upper Yellow River Basin using a modified VIC model and results showed that streamflow has decreased during recent decades. In the Kuye River Basin in Northwest China, Yang & Yang (2011) found annual runoff has declined significantly during the past 60 years. Generally, streamflow has tended to diminish and evaporation has tended to increase in many basins of northern China owing to climate change (Wang & Hejazi 2011; Wang et al. 2014, 2018b; Shen et al. 2017). However, the extent to which these basins may be resistant to climatic perturbations should be explored further with regard to the prediction of basin responses to future climate change (Xue et al. 2017).

In hydrology, the concepts of resistance and resilience, which are taken from the field of ecology, are two metrics used to quantify basin response to climate change (Zhang et al. 2001; Williams et al. 2012). In ecological studies, a resilient ecosystem is defined as one that has the ability to absorb change induced by external factors and retain its ecological function (Creed et al. 2014). In recent years, this concept has been applied in hydrological sciences (Trenbath 1999; Gerten et al. 2005). The concept of hydrological resilience is described as the capability of a basin to maintain stability in multiple hydrological equilibrium states. Creed et al. (2014) found that climate warming was projected to change forest runoff, so he calculated the resilience and resistance of 12 watersheds across North America and concluded that the forest type is the dominant factor affecting the elasticity of a specific watershed. Helman et al. (2017) calculated these two metrics of forests in the Eastern Mediterranean and found that a drier climate may induce higher resilience compared with a more humid climate. Therefore, these two metrics have been applied and to some extent can reflect the characteristics of the river basin following the climate change. In this study, we used the Budyko theoretical curve to describe the relationship between basin resilience and climate change (Shen et al. 2017). The Budyko curve, which comprises a dryness index (DI = PET/P) and an evaporative index (EI = AET/P), describes the relationship between potential evaporation and actual evaporation (Troch et al. 2013). The Budyko curve defines two basin states with evaporation being limited by either energy supply or water supply, which is determined by the calculated value of the DI (Figure 1). A value of DI <1 indicates an energy-limited basin, whereas a value of DI >1 indicates a water-limited basin. Based on

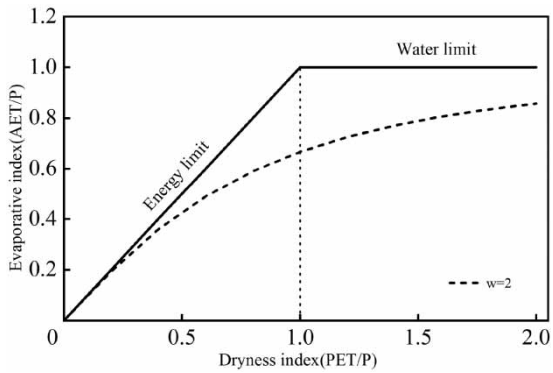

Figure 1 | The Budyko theoretical curve. The horizontal coordinate is the dryness index (DI = PET/P) and the vertical coordinate is the evaporative index (EI = AET/P). The solid line represents two different basin states, i.e. the energy and water limitations to the EI, and the dashed line represents the theoretical Budyko curve.

the Budyko curve, we calculated two metrics, i.e. dynamic deviation (d) and elasticity (e), which can be used to quantify the resilience and resistance of a basin to the effects of climate change (Creed *et al.* 2014; Helman *et al.* 2017). Dynamic deviation, which is described as the vertical departure of the EI from the corresponding value calculated using the theoretical Budyko curve, represents the resistance of a basin in terms of the runoff change caused by climate change. A positive (negative) value of the dynamic deviation indicates that runoff generated is smaller (greater) than the value estimated using the Budyko theoretical equations, and its absolute magnitude reflects the extent of the runoff change relative to the inherent runoff calculated by the Budyko theoretical curve. Smaller values of the dynamic deviation indicate higher basin resistance. Elasticity is the second metric that can be used to reflect the hydrological resilience of a basin, which represents the extent to which a watershed can hold this partitioning pattern after climate perturbations. A basin with high elasticity means runoff predictions within the basin responds highly consistently with the Budyko curve, i.e. when a change in the DI results in a change in the EI, the ecological system moves along the Budyko curve.

This study investigated the upstream area of the upper Hailar River Basin, which is situated in northeastern Inner Mongolia, China. The upper Hailar River Basin is a primary tributary of the Erguna River and it is the main water source for the local industry and agriculture. Moreover, its location belongs to the ecologically vulnerable area. So it is meaningful to detect the water balance changes following the climate change and quantify its hydrological resilience and resistance to climate change for future water resource management. In this study, we employed the Mann–Kendall test to analyze the changing hydrological balance of the study basin and adopted two metrics to determine the basin's hydrological resilience, which is used as a supplement. The objective was to investigate the following: (1) the changes in hydroclimatic variables/climate in the study basin over the previous 30 years, (2) the basin response to the changes in climate and water balances variables, and (3) the resilience of the basin to climate change. The findings of this study will assist water resources management in the basin.

MATERIALS AND METHOD

Study area

The study area comprised the upper reaches of the Hailar River Basin that drains a watershed of 43,345 km^2 (Fang *et al.* 2020). This area is located in northeastern Inner Mongolia, China (47°35′–50°12′N, 118°45′–122°40′E), and it usually experiences extreme weather caused by the influence of the East Asian summer monsoon, which means it is highly sensitive to climate change (Figure 2). The river originates in the Greater Khingan Mountains and finally joins the Erguna River (Duan *et al.* 2010). The length of the main river is 708.5 km. The study area has a temperate continental monsoon climate, i.e. short cool summers and long cold winters (Fang *et al.* 2020). Mean annual precipitation and mean annual temperature in this river basin are 347.6 mm and −1.2 °C, respectively, according to observed meteorological data during 1979–2018 (www.tpedatabase.cn). The study area is 510–1,622 m above sea level and its topography is predominantly mountains, hills, and wetlands.

Standardized precipitation and evapotranspiration index

In this study, the standardized precipitation and evapotranspiration index (SPEI) was selected as the drought monitoring index. This index considers the statistical distribution of precipitation and the potential evapotranspiration at the same time and it can reflect the regional drought more comprehensively. According to Abbasi *et al.* (2019), the SPEI can be calculated as described in the following.

First, the water-year potential evapotranspiration (ET_0) is calculated using the radiation-based formulation of Priestley and Taylor (Dewes *et al.* 2017), as shown below:

$$PET = 1.26^{*}\left(\frac{\Delta}{\Delta+\gamma}\right)(R_N - G) \quad (1)$$

where R_N is net radiation, Δ is the gradient of saturated vapor pressure, G is soil heat flux, and γ is the psychrometric constant. The unit of the variable PET is mm/d. Second, the difference between monthly precipitation and evapotranspiration is calculated as $D_i = P_i - PET_i$, where i is the

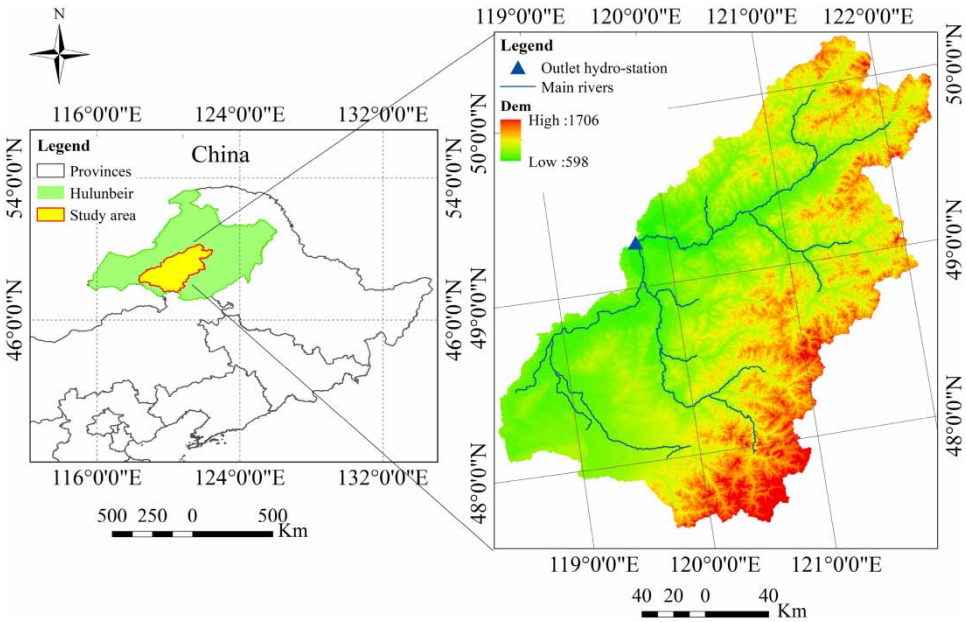

Figure 2 | Map of the study area and its position in China.

month counter. Third, the accumulation sequence of water profit and loss over different timescales is established using Equation (2), where k is the timescale (here, $k = 12$):

$$D_n^k = \sum_{i=0}^{k-1} (P_{n-i} - PET_{n-i}),\ n \geq k \tag{2}$$

Fourth, the D_n^k data series should be fitted and normalized to calculate the SPEI. Vicente-Serrano *et al.* (2010) showed that the log-logistic density function is the best fitting function to fit the D_n^k data series through contrasting the different types of parameter function. The expression of the log-logistic probability density function including three parameters is as follows:

$$f(x) = \frac{\beta}{\alpha}\left(\frac{x-\gamma}{\alpha}\right)^{\beta-1}\left[1+\left(\frac{x-\gamma}{\alpha}\right)^{\beta}\right]^{-2} \tag{3}$$

where α, β, and γ are the parameters of scale, shape, and beginning, respectively. The linear moment method is adopted to estimate the fitting parameters of this function according to the following formulas:

$$\beta = \frac{2w_1 - w_0}{(6w_1 - w_0 - 6w_2)} \tag{4}$$

$$\alpha = \frac{(w_0 - 2w_1)\beta}{\Gamma\left(1+\frac{1}{\beta}\right)\Gamma\left(1-\frac{1}{\beta}\right)} \tag{5}$$

$$\gamma = w_0 - \alpha\Gamma\left(1+\frac{1}{\beta}\right)\Gamma\left(1-\frac{1}{\beta}\right) \tag{6}$$

$$w_s = \frac{1}{n}\sum_{i=1}^{n}\left[1-\frac{l-0.35}{n}\right]^{s} \mathrm{X}_l, \tag{7}$$

where w_s is the probability weighted moment, s is taken as 0, 1, or 2, l is the sequence of accumulated water deficit X in ascending order ($\mathrm{X}_1 \leq \mathrm{X}_2, \ldots, \leq \mathrm{X}_n$), and $\Gamma(\beta)$ is the gamma function. Through the three-parameter log-logistic probability distribution function, the cumulative probability on a given timescale can be calculated using Equation (7) (Polong *et al.* 2019). Then, the SPEI is calculated using

Equation (9):

$$F(x) = \left[1 + \left(\frac{\alpha}{x - \gamma}\right)^{\beta}\right]^{-1} \tag{8}$$

$$SPEI = W - \frac{C_0 + C_1 W + C_2 W^2}{1 + d_1 W + d_2 W^2 + d_3 W^3} \tag{9}$$

where $C_0 = 2.515517$, $C_1 = 0.802853$, $C_2 = 0.010328$, $d_1 = 1.432788$, $d_2 = 0.189269$, and $d_3 = 0.001308$ (Gao *et al.* 2017). Finally, W is calculated using Equation (11):

$$P = 1 - F(x) \tag{10}$$

$$W = \begin{cases} \sqrt{-2\ln(P)} & P \le 0.5 \\ \sqrt{-2\ln(P-1)} & P > 0.5 \end{cases} \tag{11}$$

Having obtained the SPEI, a criterion was required to determine the occurrence of drought (Table 1). In this study, if the value of the SPEI was less than –0.5, we considered a drought phenomenon happened; if the value of the SPEI was positive, we considered the drought period over (Begueria *et al.* 2014).

Calculation of Budyko metrics

Based on the Budyko hypothesis, the annual water balance can be described using the function of water (precipitation) and energy (potential evaporation). Among the various forms of equations for Budyko curves, we selected the following (Zhang *et al.* 2001):

$$\frac{ET}{P} = \frac{1 + w\frac{ET_0}{P}}{1 + w\frac{ET_0}{P} + \left(\frac{ET_0}{P}\right)^{-1}} \tag{12}$$

Table 1 | Classification of the standardized precipitation evapotranspiration index

Drought categories	SPEI values
Extreme drought	≤–2.0
Severe drought	–2.0 to –1.0
Moderate drought	–1.0 to –0.5
Normal	–0.5 to 0.5
Moderate wet	0.5–1.0
Severe wet	1.0–2.0
Extreme wet	≥2.0

where P, ET, and ET_0 are mean annual precipitation, mean annual actual evaporation, and potential evapotranspiration, respectively. Parameter w is a constant determined by the characteristics of the watershed, e.g. vegetation type and soil type (Qiu *et al.* 2019). In this study, we used the adjusted equation assuming $w = 2$ to describe the theoretical relationship between the dryness index $\left(DI = \frac{ET_0}{P}\right)$ and the evaporative index $\left(EI = \frac{ET}{P}\right)$.

The parameters of deviation (d) and elasticity (e) were calculated for the studied basin to represent the potential departure from the Budyko theoretical curve of the DI and EI points (Creed *et al.* 2014). Deviation is described as the vertical departure of the EI from the corresponding B value calculated from the theoretical Budyko curve, which is composed of two parts: static and dynamic deviation. Static deviation is calculated as the mean annual EI minus its theoretical B value obtained from the mean annual DI, which is the inherent deviation with average normal climate conditions ($s = (EI_{AVG} - B)$, Figure 3). Dynamic deviation

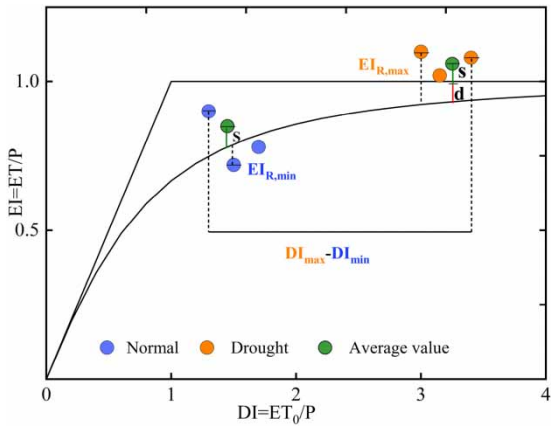

Figure 3 | Graphical representation of three Budyko metrics: static deviation (s), dynamic deviation (d), and elasticity (e). Static deviation (s) is the inherent deviation with average normal climate conditions, which is calculated as the average EI minus the B value calculated from the Budyko theoretical curve according to the mean DI under normal climate conditions ($s = (EI_N - B_N)$). Dynamic deviation (d) is the departure of the mean annual EI from the B value with climate change after considering the inherent static deviation, which is the additional deviation induced by climate change [$d = (EI_d - B_d) - s$)]. Its absolute magnitude reflects the hydrologic resistance of the basin to climate change. Elasticity (e) is the ratio of the range of the DI to the range of the residual EI, which is the magnitude of the EI departure from its corresponding B value according to the Budyko theoretical cure for the entire period [$e = (DI_{max} - DI_{min})/(EI_R max - EI_R min)$]. High elasticity indicates a basin has hydrological resilience.

(d) is the departure of the mean annual EI from the B value with climate change after considering the inherent static deviation [$d = (EI_D - B_D) - s$]. Thus, dynamic deviation is the additional deviation induced by climate change and its absolute magnitude reflects the hydrologic resistance of the basin to climate change. A value of d close to zero indicates the basin has high hydrological resistance (Helman *et al.* 2017). Elasticity (e) is defined as the ratio of the range of the DI ($DI_{max} - DI_{min}$) to the range of the EI_R ($EI_{R,}max - EI_{R,}min$), which is the magnitude of the departure of the EI from its corresponding B value according to the Budyko theoretical cure for the entire period of climate change [$e = (DI_{max} - DI_{min})/(EI_{R,}max - EI_{R,}min)$]. The points representing the DI and the EI with low departures from the Budyko curve tend to have large values of e, indicating that the basin has high elasticity, and vice versa. In addition, we used a threshold of $e = 1$ to distinguish elastic and inelastic basins. The actual evapotranspiration (ET_0) was calculated based on the water balance (Xue *et al.* 2012, 2013):

$$ET_0 = P - Q - \triangle S \tag{13}$$

where P is precipitation, R is streamflow, E is evapotranspiration, and ΔS is the change of water storage volume (Bao *et al.* 2019). We considered water storage negligible, assuming a steady state for the study period (1980–2011).

The Mann–Kendall test

The nonparametric Mann–Kendall test can be used to analyze change trends and breakpoints of hydrological time series (Sung *et al.* 2015). It can accommodate many types of samples because it does not need the samples to follow any particular distribution and it is rarely disturbed by abnormal data (Liang *et al.* 2013).

For an assumed data series X ($x_1, x_2, \cdots x_n$), n is the length of the data series. First, the cumulative statistic S should be calculated as follows:

$$S_k = \sum_{i=1}^{k} r_1 \quad k = 2, 3, \cdots n \tag{14}$$

$$r_i = \begin{cases} 1 & x_i > x_j \\ 0 & x_i \le x_j \end{cases} \quad j = 1, 2, \cdots i - 1 \tag{15}$$

where statistic S is the cumulative number of values at time i larger than at time j. Under the assumption of random independence of the time series, the statistic UF_k can be defined by the following formula:

$$UF_i = \frac{S_i - E(S_i)}{\sqrt{Var(S_i)}} \quad i = 1, 2, \cdots, n \tag{16}$$

In Equation (16), $UF_1 = 0$, and $E(S_k)$ and $Var(S_k)$ represent the expected value and the variance, respectively, of the cumulative value S_k, which can be obtained as follows:

$$E(S_i) = \frac{i(i-1)}{4} \tag{17}$$

$$Var(S_i) = \frac{i(i-1)(2i-5)}{72} \tag{18}$$

UF_i is a standard normal distribution, which is a sequence of statistics calculated from the order of time series X. Given significance level α, a condition of $|UF_i| > U_\alpha$ indicates an obvious trend change in the sequence. Using the inverse time series, we calculated the UF_i again using the above calculation process, where $UB_i = -UF_i$ and $i = n, n-1, \cdots, 1$ for the same test method as described above.

Data sources

We used daily Q data from the hydrological station at the basin outlet, which operated during 1981–2011, because we only needed annual streamflow data of the entire river basin. The daily flow was summed to an annual amount, multiplied by the corresponding length of time, and then divided by the basin area to obtain the annual streamflow.

Gridded precipitation and temperature data ($0.025 \times 0.025^\circ$) measured during 1981–2011 were collected from GHCN-Monthly datasets (www.ncdc.noaa.gov/ghcnm/v3.php) (Zhao *et al.* 2019). Net radiation data from 1981 to 2011 with 500-m spatial resolution and 30-d composite temporal resolution were downloaded from the Global Land Data Assimilation System.

RESULTS

Trends of climatic variables in the Hailar River Basin

This study found that the Hailar River Basin has become warmer and drier in recent decades, consistent with the results of Han *et al.* (2018b). During the study period, annual mean precipitation was 429.56 mm, with the highest (lowest) annual mean precipitation of 621.41 (248.31) mm in 1998 (2007). The time series of areal precipitation in the Hailar Basin showed a decreasing trend during the studied 30 years (Figure 4(a)). The multiyear annual mean precipitation was 483.83, 443.56, and 367.52 mm in 1981–1990, 1991–2000, and 2001–2011, respectively. The multiyear mean annual precipitation during 1991–2000 was 40.27 mm less than in 1981–1990 but 76.04 mm higher than in 2001–2011, which indicates that the rate of decrease of annual mean precipitation before 2000 was much smaller than after 2001. According to the P value calculated from the linear regression ($P = -0.48$), the trend of decrease of annual mean precipitation was insignificant at the $\alpha = 0.05$ level (Figure 4(a)). Moreover, the results of the Mann–Kendall test revealed an oscillation in mean annual precipitation before 1998 and after 1998, indicating that the trend of decrease of mean annual precipitation became slightly more evident (Figure 4(b)). Therefore, although the trend of decrease of mean annual precipitation was mild, the scale of the trend intensified.

During 1981–2011, average annual temperature in the study area was –1.81 °C, with the lowest (highest) average annual temperature of –3.53 °C (–0.19 °C) in 1984 (2007). There has been a trend of increase in average annual temperature over the 30-year study period (Figure 4(c)). The multiyear annual mean temperature was –2.4, –1.56 and

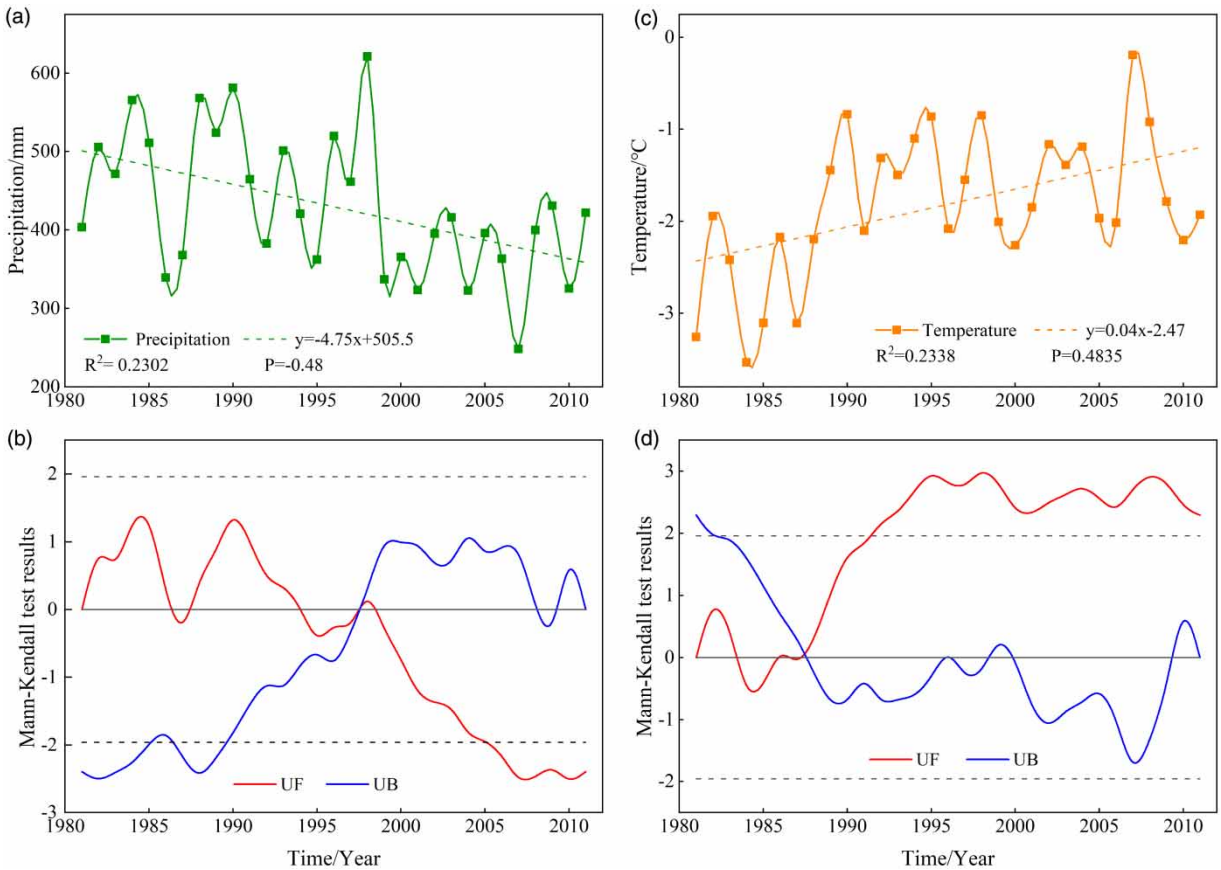

Figure 4 | Change trend of (a) annual mean precipitation and (b) annual mean temperature in the Hailar River Basin during 1981–2011. Mann–Kendall test results for (c) precipitation and (d) temperature (red line: calculated UF value, blue line: calculated UB value). Please refer to the online version of this paper to see this figure in colour: http://dx.doi.org/10.2166/nh.2020.032.

–1.51 °C in 1981–1990, 1991–2000, and 2001–2011, respectively. The multiyear mean annual temperature during 1991–2000 was 0.84 °C higher than in 1981–1990 but 0.04 °C lower than in 2001–2011, which indicates that the rate of increase in temperature has decreased slightly in comparison with earlier years. Statistically, the P value ($P = 0.4835$) calculated from the linear regression indicates that this trend of increase was not significant and that its process of change was uncertain (Figure 4(c)). In addition, according to the results of the Mann–Kendall test, the trend of increase in annual mean temperature was significant after 1993 at the $\alpha = 0.05$ level. Generally, despite the uncertain trend of change of temperature, it was clearer than that of precipitation (Figure 4(d)).

We also analyzed the change of humid/dry climate in the Hailar River Basin based on the SPEI. It was found that drought intensified during the study period, especially during 1998–2011 (Figure 5). The variations of the 12-month SPEI and the Mann–Kendall test results of the SPEI for the Hailar River Basin during 1981–2011 are shown in Figure 5. The general trend of decrease indicates that this area has experienced increasing occurrence and intensification of drought. The maximum (minimum) SPEI of 2.76 (–2.69) was in 2007 (1998), which was the wettest (driest) year in the study period. The UF curve shows that

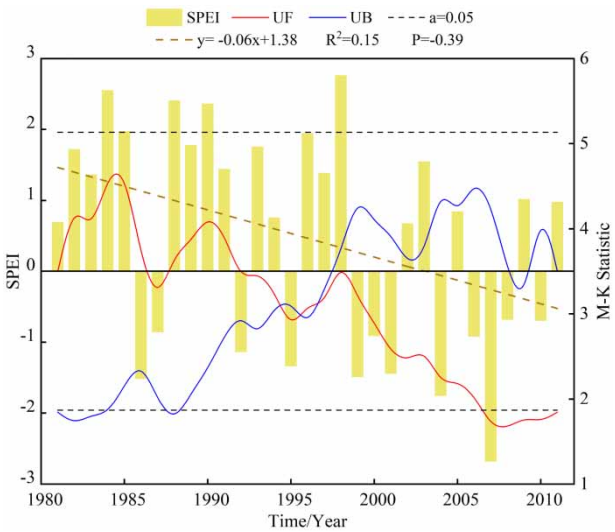

Figure 5 | Variation of the calculated annual SPEI and the Mann–Kendall test results of the SPEI in the upper Hailar River Basin during 1981–2011 (red line: calculated UF value, blue line: calculated UB value). Please refer to the online version of this paper to see this figure in colour: http://dx.doi.org/10.2166/nh.2020.032.

the SPEI in the Hailar River Basin has risen and fallen during the 30-year study period. During 1981–1991 (except 1987), the UF value was positive, indicating that the value of the SPEI showed an overall trend of rise during this period. During 1992–2011 (except 1993 and 1998), the UF value was <0 and it exceeded the confidence interval of 0.05 after 2007, showing that the SPEI decreased gradually and that the change trend of the SPEI was significant after 2007. Within the confidence interval, the UF and UB curves intersect in 1998, indicating that 1998 was the breakpoint of the SPEI and that drought has intensified in the Hailar River Basin since 1998 (Zhai *et al.* 2010).

Water balance change in the Hailar River Basin

The water balance of the Hailar River Basin has changed during the study period (Figure 6). During 1981–2011, annual mean runoff at the outlet hydrological station has decreased at the rate of 1.46 mm/year (Figure 6(a)). The change trend of annual mean runoff was similar to that of precipitation (Figure 4(a)). During 1981–1990, 1991–2000, and 2001–2011, annual mean runoff was 102.26, 86.88, and 52.51 mm, respectively. Annual mean runoff during 1991–2000 was 15.38 mm lower than in 1981–1990 but 34.37 mm higher than in 2001–2011. Therefore, the rate of annual mean runoff decrease was increased during the study period. As shown in Figure 6(a), 1998 represents the breakpoint of the annual mean runoff series. Prior to 1998, repeated oscillation occurred in the time series of annual mean runoff, whereas annual mean runoff showed a more obvious decreasing trend after 1998. Throughout the entire data series, the decreasing trend of annual runoff was insignificant at the $\alpha = 0.05$ level, according to the obtained P value ($P = -0.53$). In addition, annual mean evaporation has decreased generally during the 30-year study period with a change trend similar to but more evident than that of annual mean runoff (Figure 6(b)). However, the rate of decrease of annual mean evaporation has been smaller than the change trend of precipitation.

The proportions of precipitation allocated to runoff and evaporation have also changed during the study period, i.e. a smaller proportion of precipitation has generated runoff, while a greater proportion has been evaporated. As shown in Figure 7, there has been a general trend of decrease in

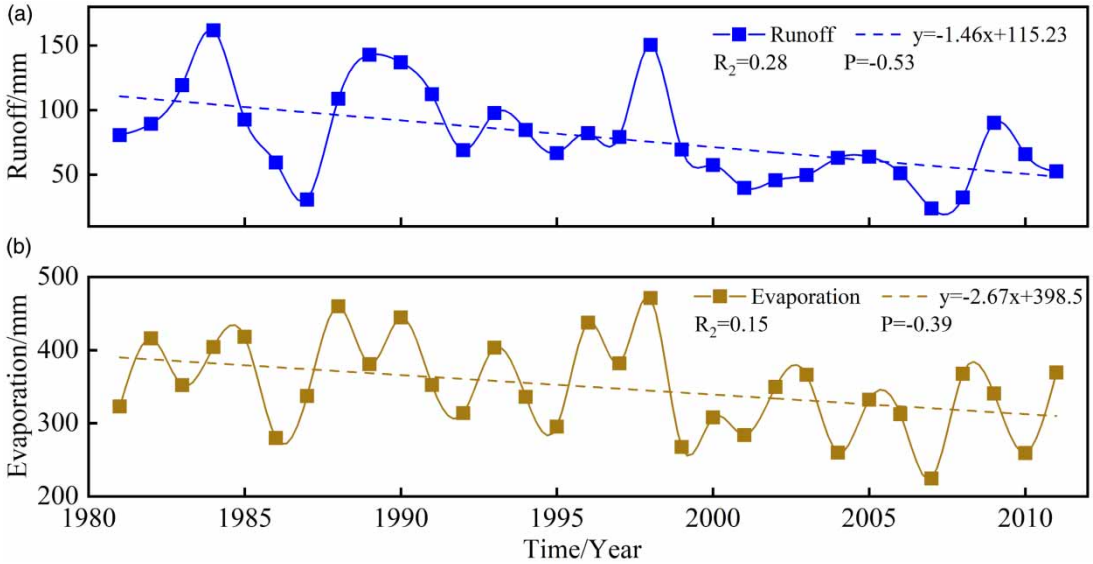

Figure 6 | Change trends of hydrological variables in the upper Hailar River Basin in the studied 30 years: (a) runoff and (b) evaporation.

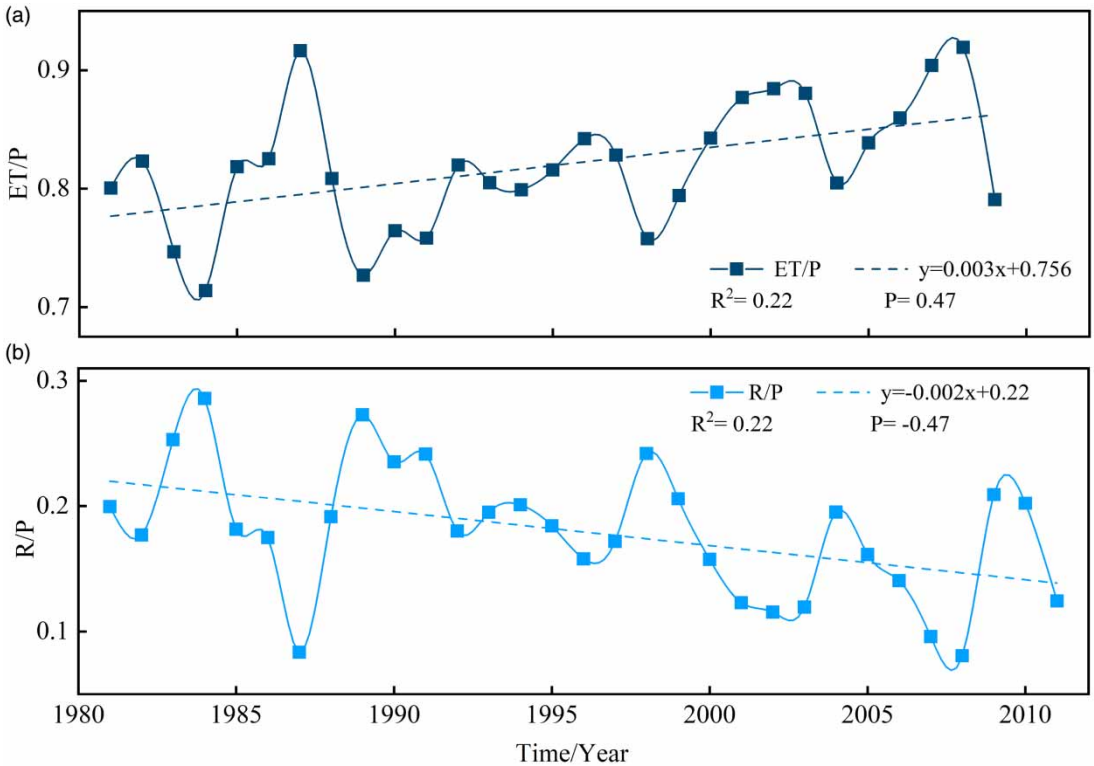

Figure 7 | Change trends of (a) ET/P and (b) R/P during 1981–2011.

the runoff–precipitation ratio and a trend of increase in the evaporation–precipitation ratio. The multiyear mean runoff–precipitation ratio was 0.206, 0.194, and 0.143 during 1981–1990, 1991–2000, and 2001–2011, respectively. It is evident that there was no change in the relationship between precipitation and runoff during 1981–2000, i.e.

the runoff–precipitation ratio during 1991–2000 was 0.012 higher than during 1981–1990, which indicates that the same percentage of runoff was generated at this time. However, there was a significant decrease in the runoff–precipitation ratio after 2000, i.e. the decrease of 0.051 during 2001–2011 relative to 1991–2000 indicates less precipitation was converted into runoff. The change trend of the runoff–precipitation ratio was consistent with the trend of annual mean runoff.

Resistance and resilience of the watershed

Based on the calculated SPEI, we calculated five-year moving averages for the period 1981–2011. Finally, we selected 1981–1985 as the wet period with maximum average values of the SPEI and 2004–2008 as the dry period with minimum average values of the SPEI (Figure 8). According to the DI and EI in the normal climate period, s was calculated using the equation described in the above. An obtained value of $s < 0$ indicated that runoff generated in the five-year wet period was larger than the predicted runoff based on the Budyko curve, and vice versa. Obtained points distributed near the Budyko theoretical curve ($|s| < 0.05$) indicated the pre-warming runoff fitted the predicted values using the Budyko curve, which reflected the inherent characteristics of the basin. The value of s calculated for the Hailar River Basin was 0.035, i.e. a positive value whose absolute value is within the scope of 0.05. It reflects that pre-warming runoff produced under a normal climate was smaller than the runoff predicted using the Budyko curve, although it was very close to the theoretical runoff.

Dynamic deviation (d) describes the vertical departure of points (DI, EI) in the five-year dry period from the Budyko curve when considering the static deviation. Its absolute magnitude reflects the hydrological resistance of the basin to climate change, according to runoff change, in comparison with the runoff estimated using the Budyko curve. In the Hailar River Basin, the calculated value of d was –0.0183, which is less than zero and indicates higher runoff than estimated according to the Budyko curve. Moreover, the absolute value of d was close to zero, which shows the extent of runoff change has been small under the effects of climate change, reflecting high hydrological resistance of the basin to climate change.

The hydrological resilience of a basin is reflected by its elasticity (e). In a basin with high elasticity, runoff change under the effects of climate change is consistent with the Budyko curve. For example, as can be seen from Figure 8, when change in the DI results in change of the EI along the Budyko curve, the basin has hydrological resilience (Trenbath 1999). Conversely, change in the DI that leads to change in the EI that deviates from the Budyko curve reflects a basin without hydrological resilience. The value of elasticity we calculated was 8.03, which is much greater than 1 and reflects the high hydrological resilience of the Hailar River Basin.

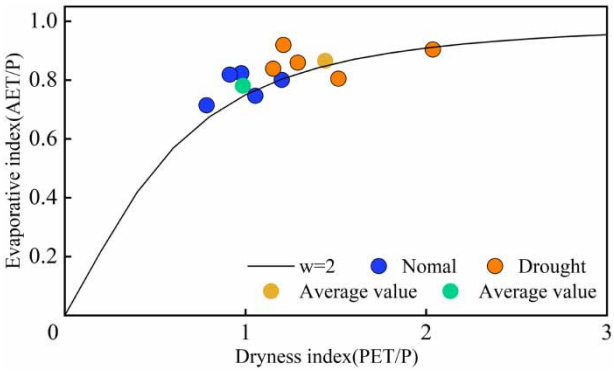

Figure 8 | Distribution of 10 points chosen from the 30-year study period according to the SPEI in the Budyko theoretical framework.

DISCUSSION

During 1981–2011 in the Hailar River Basin, there was a trend of decrease in annual mean precipitation and a trend of increase in annual mean temperature (Figure 4). As the calculated results showed, the rate of decrease of precipitation and the rate of increase of temperature both increased gradually to some degree, indicating that the climate of the upper Hailar River Basin during the studied 30-year period has changed and that this change might become intensified in the future (Figure 4). Moreover, the observed decreased precipitation and increased temperature are projected to lead to intensification of drought, consistent with the results of Wang *et al.* (2014). This type of

phenomenon is consistent with that observed in the region of the Hulunbuir grassland during 1960–2017 (Wang *et al.* 2018b).

Under the background of climate change, the water balance in the upper Hailar River Basin has changed. Annual mean runoff has shown a decreasing trend during the study period (Figure 6(b)), consistent with the simulated results (Duan *et al.* 2010). Precipitation is the origin of runoff generation and the decrease of precipitation induced the reduction of runoff. In addition, a greater proportion of precipitation is now evaporated and less transformed into runoff (Figure 7(a) and 7(b)). However, annual mean evaporation also shown a decreasing trend due to the substantial decrease of precipitation. Owing to the increase of temperature, a greater proportion of precipitation is now evaporated (Han *et al.* 2018a). In addition, increased vegetation coverage has led to a greater uptake of water and enhanced evapotranspiration (Zhao *et al.* 2014; Fang *et al.* 2018a; Bao *et al.* 2019). Thus, the proportion of precipitation converted to runoff has been reduced and the amount of runoff has declined.

In our study, the calculated values of d and e were –0.0183 and 8.03, respectively. The values of these two metrics reflect the high level of hydrological resistance and resilience of the Hailar River Basin, confirming that the predicted runoff change has high consistency with the Budyko curve. The obtained value of $e > 1$ indicates that the change in the DI during the entire study period was greater than the change in the EI (Creed *et al.* 2014). Several of the factors that contribute to high elasticity were analyzed and among the dominant influencing hydrological factors were those that contribute to certain changes in ET_0. For example, seasonal precipitation has an effect on the evaporative indices based on the Budyko framework (Gentine *et al.* 2012; Williams *et al.* 2012). Annual precipitation in the Hailar River Basin (30–350 mm) is concentrated primarily in summer (Fang *et al.* 2018a). Given the high temperature and large quantity of precipitation in summer, potential evaporation in this water-limited area is maximized and the range of the DI is increased. Additionally, Klein *et al.* (2013) argued that some basins can adjust their own ecophysiological factors to cope with drought induced by climate change, such as WUE (Xue *et al.* 2016; Yao *et al.* 2020). Therefore, water use efficiency in the basin is large (small) in the dry (wet) period (Xue *et al.* 2015; Han *et al.* 2018a; Sun *et al.* 2020). This flexibility of water use efficiency in different periods increased the basin's ability to cope with climate change and further enhanced the hydrological resilience of the basin to climate change (Ponce-Campos *et al.* 2013).

CONCLUSIONS

In the Hailar River Basin, the major features of climate change during the 30-year study period (1981–2011) are represented by increased temperature, decreased precipitation, and intensified drought. We used the Mann–Kendall test to investigate the water balance changes in this basin based on certain hydrological variables, e.g. precipitation and runoff. Based on hydrological data obtained during the study period, it was determined that the water balance change has been manifest as trends of decrease of runoff and evaporation. In addition, we used two Budyko metrics to quantify the resistance and resilience of runoff in this basin to the effects of climate change. The results showed the basin has high hydrological resilience and resistance and that it could retain its ecological function in a changing climate.

ACKNOWLEDGEMENTS

This study was supported by the National Natural Science Foundation of China (Grant 31670451) and the Fundamental Research Funds for the Central Universities (No. 2017NT18). We thank James Buxton MSc from Liwen Bianji, Edanz Group China (www.liwenbianji.cn./ac), for editing the English text of this manuscript.

DATA AVAILABILITY STATEMENT

All relevant data are included in the paper or its Supplementary Information.

REFERENCES

A, Y., Wang, G., Liu, T., Xue, B. & Kuczera, G. 2019a Spatial variation of correlations between vertical soil water and

evapotranspiration and their controlling factors in a semi-arid region. *J. Hydrol.* **574**, 53–63.

A, Y., Wang, G. Q., Liu, T. X., Shrestha, S., Xue, B. L. & Tan, Z. X. 2019b Vertical variations of soil water and its controlling factors based on the structural equation model in a semi-arid grassland. *Sci. Total Environ.* **691**, 1016–1026.

Abbasi, A., Khalili, K., Behmanesh, J. & Shirzad, A. 2019 Drought monitoring and prediction using SPEI index and gene expression programming model in the west of Urmia Lake. *Theor. Appl. Climatol.* **138**, 553–567.

Bao, Z., Zhang, J., Wang, G., Chen, Q., Guan, T., Yan, X., Liu, C., Liu, J. & Wang, J. 2019 The impact of climate variability and land use/cover change on the water balance in the Middle Yellow River Basin, China. *J. Hydrol.* **577**, 123942. https://doi.org/10.1016/j.jhydrol.2019.123942.

Begueria, S., Vicente-Serrano, S. M., Reig, F. & Latorre, B. 2014 Standardized precipitation evapotranspiration index (SPEI) revisited: parameter fitting, evapotranspiration models, tools, datasets and drought monitoring. *Int. J. Climatol.* **34**, 3001–3023.

Creed, I. F., Spargo, A. T., Jones, J. A., Buttle, J. M., Adams, M. B., Beall, F. D., Booth, E. G., Campbell, J. L., Clow, D., Elder, K., Green, M. B., Grimm, N. B., Miniat, C., Ramlal, P., Saha, A., Sebestyen, S., Spittlehouse, D., Sterling, S., Williams, M. W., Winkler, R. & Yao, H. 2014 Changing forest water yields in response to climate warming: results from long-term experimental watershed sites across North America. *Global Change Biol.* **20**, 3191–3208.

Cuo, L., Zhang, Y., Gao, Y., Hao, Z. & Cairang, L. 2013 The impacts of climate change and land cover/use transition on the hydrology in the upper Yellow River Basin, China. *J. Hydrol.* **502**, 37–52.

Dai, A. 2011 Drought under global warming: a review. *Clim. Change* **2**, 45–65.

Dewes, C. F., Rangwala, I., Barsugli, J. J., Hobbins, M. T. & Kumar, S. 2017 Drought risk assessment under climate change is sensitive to methodological choices for the estimation of evaporative demand. *PLoS One* **12**, e0174045.

Duan, L., Liu, T., Wang, X., Luo, Y. & Wu, L. 2010 Development of a regional regression model for estimating annual runoff in the Hailar River Basin of China. *J. Water Resour. Prot.* **2**, 934–943.

Fang, Q., Wang, G., Liu, T., Xue, B.-L. & Aa, Y. 2018a Controls of carbon flux in a semi-arid grassland ecosystem experiencing wetland loss: vegetation patterns and environmental variables. *Agric. For. Meteorol.* **259**, 196–210.

Fang, Q., Wang, G., Xue, B., Liu, T. & Kiem, A. 2018b How and to what extent does precipitation on multi-temporal scales and soil moisture at different depths determine carbon flux responses in a water-limited grassland ecosystem? *Sci. Total Environ.* **635**, 1255–1266.

Fang, Q., Wang, G., Liu, T., Xue, B., Sun, W. & Shrestha, S. 2020 Unraveling the sensitivity and nonlinear response of water use efficiency to the water–energy balance and underlying surface condition in a semiarid basin. *Sci. Total Environ.* **699**, 134405. https://doi.org/10.1016/j.scitotenv.2019.134405.

Gao, X., Zhao, Q., Zhao, X., Wu, P., Pan, W., Gao, X. & Sun, M. 2017 Temporal and spatial evolution of the standardized precipitation evapotranspiration index (SPEI) in the Loess Plateau under climate change from 2001 to 2050. *Sci. Total Environ.* **595**, 191–200.

Gentine, P., D'Odorico, P., Lintner, B. R., Sivandran, G. & Salvucci, G. 2012 Interdependence of climate, soil, and vegetation as constrained by the Budyko curve. *Geophysical Research Letters* **39**, L19404. http://doi.org/10.1029/2012gl053492.

Gerten, D., Lucht, W., Schaphoff, S., Cramer, W., Hickler, T. & Wagner, W. 2005 Hydrologic resilience of the terrestrial biosphere. *Geophys. Res. Lett.* **32**, L21408. https://doi.org/10.1029/2005GL024247.

Han, D., Wang, G., Liu, T., Xue, B.-L., Kuczera, G. & Xu, X. 2018a Hydroclimatic response of evapotranspiration partitioning to prolonged droughts in semiarid grassland. *J. Hydrol.* **563**, 766–777.

Han, D., Wang, G., Xue, B., Liu, T., Y, A. & Xu, X. 2018b Evaluation of semiarid grassland degradation in North China from multiple perspectives. *Ecol. Eng.* **112**, 41–50.

He, B., Miao, C. Y. & Shi, W. 2013 Trend, abrupt change, and periodicity of streamflow in the mainstream of Yellow River. *Environ. Monit. Assess.* **185**, 6187–6199.

Helman, D., Lensky, I. M., Yakir, D. & Osem, Y. 2017 Forests growing under dry conditions have higher hydrological resilience to drought than do more humid forests. *Glob. Chang. Biol.* **23**, 2801–2817.

Klein, T., Di Matteo, G., Rotenberg, E., Cohen, S. & Yakir, D. 2013 Differential ecophysiological response of a major Mediterranean pine species across a climatic gradient. *Tree Physiol.* **33**, 26–36.

Liang, L. Q., Li, L. J., Liu, C. M. & Cuo, L. 2013 Climate change in the Tibetan Plateau Three Rivers Source Region: 1960–2009. *Int. J. Climatol.* **33**, 2900–2916.

Miao, L., Jiang, C., Xue, B., Liu, Q., He, B., Nath, R. & Cui, X. 2014 Vegetation dynamics and factor analysis in arid and semi-arid Inner Mongolia. *Environ. Earth Sci.* **73**, 2343–2352.

Polong, F., Chen, H., Sun, S. & Ongoma, V. 2019 Temporal and spatial evolution of the standard precipitation evapotranspiration index (SPEI) in the Tana River Basin, Kenya. *Theor. Appl. Climatol.* **138**, 777–792.

Ponce-Campos, G. E., Moran, M. S., Huete, A., Zhang, Y., Bresloff, C., Huxman, T. E., Eamus, D., Bosch, D. D., Buda, A. R., Gunter, S. A., Scalley, T. H., Kitchen, S. G., McClaran, M. P., McNab, W. H., Montoya, D. S., Morgan, J. A., Peters, D. P. C., Sadler, E. J., Seyfried, M. S. & Starks, P. J. 2013 Ecosystem resilience despite large-scale altered hydroclimatic conditions. *Nature* **494**, 349–352.

Qiu, H., Niu, J. & Phanikumar, M. S. 2019 Quantifying the space–time variability of water balance components in an agricultural basin using a process-based hydrologic model and the Budyko framework. *Sci. Total Environ.* **676**, 176–189.

Shen, Q., Cong, Z. & Lei, H. 2017 Evaluating the impact of climate and underlying surface change on runoff within the Budyko framework: a study across 224 catchments in China. *J. Hydrol.* **554**, 251–262.

Sun, W., Jin, Y., Yu, J., Wang, G., Xue, B., Zhao, Y., Fu, Y. & Shrestha, S. 2020 Integrating satellite observations and human water use data to estimate changes in key components of terrestrial water storage in a semi-arid region of North China. *Sci. Total Environ.* **698**, 134171. https://doi.org/10.1016/j.scitotenv.2019.134171.

Sung, J. H., Chung, E.-S., Kim, Y. & Lee, B.-R. 2015 Meteorological hazard assessment based on trends and abrupt changes in rainfall characteristics on the Korean peninsula. *Theor. Appl. Climatol.* **127**, 305–326.

Trenbath, B. R. 1999 Multispecies cropping systems in India – predictions of their productivity, stability, resilience and ecological sustainability. *Agrofor. Syst.* **45**, 81–107.

Troch, P. A., Carrillo, G., Sivapalan, M., Wagener, T. & Sawicz, K. 2013 Climate-vegetation-soil interactions and long-term hydrologic partitioning: signatures of catchment co-evolution. *Hydrol. Earth Syst. Sci.* **17**, 2209–2217.

Vicente-Serrano, S. M., Beguería, S. & López-Moreno, J. I. 2010 A multiscalar drought index sensitive to global warming: the standardized precipitation evapotranspiration index. *J. Clim.* **23**, 1696–1718.

Wang, D. & Hejazi, M. 2011 Quantifying the relative contribution of the climate and direct human impacts on mean annual streamflow in the contiguous United States. *Water Resour. Res.* **47**, W00J12. https://doi.org/10.1029/2010WR010283.

Wang, G., Yang, H., Wang, L., Xu, Z. & Xue, B. 2014 Using the SWAT model to assess impacts of land use changes on runoff generation in headwaters. *Hydrol. Process.* **28**, 1032–1042.

Wang, G., Hu, X., Zhu, Y., Jiang, H. & Wang, H. 2018a Historical accumulation and ecological risk assessment of heavy metals in sediments of a drinking water lake. *Environ. Sci. Pollut. Res. Int.* **25** (24), 882–24,894.

Wang, G., Liu, S., Liu, T., Fu, Z., Yu, J. & Xue, B. 2018b Modelling above-ground biomass based on vegetation indexes: a modified approach for biomass estimation in semi-arid grasslands. *Int. J. Remote Sens.* **40**, 3835–3854.

Wang, G., Li, J., Sun, W., Xue, B., Y, A. & Liu, T. 2019a Non-point source pollution risks in a drinking water protection zone based on remote sensing data embedded within a nutrient budget model. *Water Res.* **157**, 238–246.

Wang, P. Z., Yao, J. P., Wang, G. Q., Hao, F. H., Shrestha, S., Xue, B. L., Xie, G. & Peng, Y. B. 2019b Exploring the application of artificial intelligence technology for identification of water pollution characteristics and tracing the source of water quality pollutants. *Sci. Total Environ.* **693**. UNSP 133440, https://doi.org/10.1016/j.scitotenv.2019.07.246.

Williams, C. A., Reichstein, M., Buchmann, N., Baldocchi, D., Beer, C., Schwalm, C., Wohlfahrt, G., Hasler, N., Bernhofer, C., Foken, T., Papale, D., Schymanski, S. & Schaefer, K. 2012 Climate and vegetation controls on the surface water balance: synthesis of evapotranspiration measured across a global network of flux towers. *Water Resour. Res.* **48**, W06523. https://doi.org/10.1029/2011WR011586.

Xue, B.-L., Komatsu, H., Kumagai, T. O., Kotani, A., Otsuki, K. & Ohta, T. 2012 Interannual variation of evapotranspiration in an eastern Siberian larch forest. *Hydrol. Process.* **26**, 2360–2368.

Xue, B.-L., Wang, L., Li, X., Yang, K., Chen, D. & Sun, L. 2013 Evaluation of evapotranspiration estimates for two river basins on the Tibetan Plateau by a water balance method. *J. Hydrol.* **492**, 290–297.

Xue, B.-L., Guo, Q., Otto, A., Xiao, J., Tao, S. & Li, L. 2015 Global patterns, trends, and drivers of water use efficiency from 2000 to 2013. *Ecosphere* **6**. UNSP 174, http://dx.doi.org/10.1890/ES14-00416.1.

Xue, B.-L., Guo, Q., Gong, Y., Hu, T., Liu, J. & Ohta, T. 2016 The influence of meteorology and phenology on net ecosystem exchange in an eastern Siberian boreal larch forest. *J. Plant Ecol.* **9**, 520–530.

Xue, B.-L., Guo, Q., Hu, T., Xiao, J., Yang, Y., Wang, G., Tao, S., Su, Y., Liu, J. & Zhao, X. 2017 Global patterns of woody residence time and its influence on model simulation of aboveground biomass. *Glob. Biogeochem. Cycles* **31**, 821–835.

Yang, H. & Yang, D. 2011 Derivation of climate elasticity of runoff to assess the effects of climate change on annual runoff. *Water Resour. Res.* **47**. UNSP 174, https://doi.org/10.1029/2010WR009287.

Yao, J. P., Wang, P. Z., Wang, G. Q., Shrestha, S. G., Xue, B. L. & Sun, W. C. 2020 Establishing a time series trend structure model to mine potential hydrological information from hydrometeorological time series data. *Sci. Total Environ.* **698**, 134227. https://doi.org/10.1016/j.scitotenv.2019.134227.

Zhai, J. Q., Liu, B., Hartmann, H., Su, B. D., Jiang, T. & Fraedrich, K. 2010 Dryness/wetness variations in ten large river basins of China during the first 50 years of the 21st century. *Quat. Int.* **226**, 101–111.

Zhang, L., Dawes, W. R. & Walker, G. R. 2001 Response of mean annual evapotranspiration to vegetation changes at catchment scale. *Water Resour. Res.* **37**, 701–708.

Zhang, Y., Pena-Arancibia, J. L., McVicar, T. R., Chiew, F. H., Vaze, J., Liu, C., Lu, X., Zheng, H., Wang, Y., Liu, Y. Y., Miralles, D. G. & Pan, M. 2016 Multi-decadal trends in global terrestrial evapotranspiration and its components. *Sci. Rep.* **6**, 19124. https://doi.org/10.1038/srep19124.

Zhao, G. J., Tian, P., Mu, X. M., Jiao, J. Y., Wang, F. & Gao, P. 2014 Quantifying the impact of climate variability and human activities on streamflow in the middle reaches of the Yellow River basin, China. *J. Hydrol.* **519**, 387–398.

Zhao, H., Huang, W., Xie, T., Wu, X., Xie, Y., Feng, S. & Chen, F. 2019 Optimization and evaluation of a monthly air temperature and precipitation gridded dataset with a 0.025° spatial resolution in China during 1951–2011. *Theor. Appl. Climatol.* **138**, 491–507.

First received 9 March 2020; accepted in revised form 15 May 2020. Available online 7 July 2020